

MIXING OF A JET IN A PIPE

Mikael Mortensen, Wojciech Orciuch, Mounir Bouaifi, Bengt Andersson
Chalmers University of Technology, Department of Chemical Reaction Engineering, 412 96
Gothenburg, Sweden
CFD, PDF, PLIF, scalar mixing

SUMMARY

Planar laser induced fluorescence measurements were performed on a passive tracer coaxially injected in the center of a larger pipe carrying intermediate to fully turbulent flows. Axial distributions of mean concentration and concentration variance for the tracer are presented. Results were compared with theoretical predictions of two multiple-time-scale models for concentration variance. Calculations were performed with computational fluid dynamics. Finally concentration distributions were compared to beta-PDFs.

INTRODUCTION

Turbulent mixing is central to the understanding of reactive flows, and to the calculations of selectivity, product quality and yield of fast chemical reactions in turbulent flows. Most currently employed models for scalar mixing, ranging from simple moment closures to full probability density function (PDF) methods, require information concerning the coupling between the turbulence time scale and the scalar dissipation time scale for closure. This information is provided by the turbulent mixer model of Ba³dyga¹ and the spectral relaxation model of Fox², which are both multiple-time-scale mixing models for the concentration variance of a passive scalar. From the first two moments of the concentration it is then possible to get a presumed, continuous or discrete, PDF. The beta-function, as presumed continuous PDF, was verified and recommended by Rhodes³, Frankel, Madnia et al.⁴ and Madnia, Frankel et al.⁵ and is commonly used in chemical reaction rate closures (Li and Toor⁶, Ba³dyga¹, Bilger⁷).

The purpose of the present study is to compare the multi-scale models to experiments performed with Planar laser induced fluorescence (PLIF) in a pipe. PLIF is a very attractive non-intrusive experimental technique for studying concentration distributions of a passive tracer. Earlier it has been successfully applied in for example describing mixing in stirred tanks (Houcine, Marcant et al.⁸, Houcine, Vivier et al.⁹) and numerous other applications in reacting and non-reacting, gaseous and liquid flows (Eckbreth¹⁰). The current work applies a coaxial injection pipe in the centre of a larger tube. Intermediate and fully turbulent flows are used in the large tube, whereas the flow in the injection pipe is laminar. Coaxial injection in a larger tube has earlier been extensively reported in the literature. Guiraud, Bertrand et al.¹¹ presents a thorough experimental study for both velocity and concentration, but for high Reynolds numbers (>40000) of the injection pipe and low Reynolds number in the main flow. No PDFs for the concentration were reported. Kruis and Falk¹² report rather large deviations between the multi-scale models and the experimental data of Guiraud et al.¹¹. Ba³dyga and Henczka¹³, Heinz and Roekaerts¹⁴ and Ba³dyga and Orciuch¹⁵ report on the effect of Reynolds number on mixing and thereby the selectivity of chemical reactions or the quality of precipitation products. These last three works employ the same system geometry as the current work and also keep the injection flow laminar and the main flow turbulent. However, no direct experimental validation of the mixing models was reported.

PLANAR LASER INDUCED FLUORESCENCE

Planar laser induced fluorescence (PLIF) is a non-intrusive technique for measuring concentration fields of a fluorescent compound in liquids or gases. PLIF involves a laser, a fast CCD-camera, a fluorescent tracer and a computer for gathering digital images. A laser beam is passed through a prism, a cylindrical lens and a plano-convex lens to produce a thin planar laser sheet. When this sheet is passed through a liquid containing a fluorescent tracer, a photon from the laser will excite a tracer molecule whenever the two meet. The excited molecule will quickly fall off to a lower energy state and in this process a photon of a certain wavelength is emitted. A camera can capture the emitted light and the amount of light captured (fluorescence intensity) is thus a measure of the number of excited molecules. The relationship between fluorescence intensity and concentration of tracer can be given as

$$I = \Gamma_1 C e^{(-\Gamma_2 C)} \quad (1)$$

where I is the fluorescence intensity, Γ_1 a local coefficient related to the experiment, Γ_2 a coefficient which takes into account the effects of absorption and C the tracer concentration. From equation (1) it can be seen that as long as the absorption is low the exponential term is approximately one and there is a linear relationship between fluorescence intensity and the local concentration. To obtain accurate statistics care must be taken to stay within the linear regime for all measuring points. PLIF can be used both to study turbulent structures and turbulent statistics. With a fast camera it is possible to follow a turbulent eddy as it evolves in a turbulent field. More interesting for the current work is point statistics as this can be directly compared to the multiple-time-scale models. It is then necessary to capture enough images to obtain a reasonably smooth concentration distribution. A major drawback of using PLIF in measuring turbulent statistics is that the sheet must have a certain thickness that is larger than the smallest relevant turbulence scales (the Batchelor scale). This makes it impossible to extract information at high wave numbers and thus fine-scale variance cannot be detected. However, the mean fields that are extracted should be highly accurate. Other more or less important possible sources of error that need to be considered for all PLIF experiments are instabilities of the laser intensity, instabilities in the CCD-array, background noise and, for the current work, impurities in the plexiglass tube and the box surrounding the tube.

MULTIPLE-TIME-SCALE MODELS

The turbulent mixer model (TMM) of Ba³dyga¹ and the spectral relaxation model (SRM) of Fox² are both multiple-time-scale mixing models for concentration variance. This means that more than one time-scale is employed in describing the scalar dissipation of concentration variance. An attractive feature, which is a direct consequence of the multiple scales, is that the integral length-scales of turbulence and the scalar fields need not be the same at the injection point. Thus a multi-scale model should perform well for the current system of a small injection pipe within a larger tube. The models must be solved together with an appropriate model for the turbulent velocity field. This is discussed further in the numerical simulation chapter.

The dimensionless concentration of a passive tracer, f , is governed by the following transport equation in turbulent incompressible flows:

$$\frac{Df}{Dt} = \frac{\partial}{\partial x_i} \left[D_M \frac{\partial f}{\partial x_i} \right] \quad (2)$$

Reynolds averaging and introducing the concept of turbulent diffusion yields the mean concentration equation

$$\frac{D\langle f \rangle}{Dt} = \frac{\partial}{\partial x_i} \left[(D_M + D_T) \frac{\partial \langle f \rangle}{\partial x_i} \right] \quad (3)$$

The process of mixing on the molecular scale is interpreted as dissipation of the scalar concentration variance

$$\sigma_s^2 = \langle (f')^2 \rangle = \langle (f - \langle f \rangle)^2 \rangle \quad (4)$$

Reynolds averaging of eq. (2) multiplied by f' yields the equation for the mean-square concentration fluctuations for the scalar

$$\frac{D\langle (f')^2 \rangle}{Dt} = \frac{\partial}{\partial x_i} \left[(D_M + D_T) \frac{\partial \langle (f')^2 \rangle}{\partial x_i} \right] + 2D_T \left(\frac{\partial \langle f \rangle}{\partial x_i} \frac{\partial \langle f \rangle}{\partial x_i} \right) - 2\langle \mathbf{e}_f \rangle \quad (5)$$

where the scalar dissipation is given by

$$\langle \mathbf{e}_f \rangle = D_M \left\langle \frac{\partial f'}{\partial x_i} \frac{\partial f'}{\partial x_i} \right\rangle \quad (6)$$

D_M is the molecular diffusion coefficient, $D_T = \mu_T / Sc_T$ is the turbulent diffusion coefficient, where the turbulent viscosity, μ_T , is calculated by the turbulence model. The turbulent Schmidt number, $Sc_T = 0.7$, is set as recommended by Ba³dyga and Bourne¹⁶ for round jets. The multi-scale models aim to model the scalar dissipation, which is the last unclosed term in the equation set. Details of the two models can be found in Ba³dyga¹ and Fox². A brief summary of the equations to be solved is given below.

THE TURBULENT MIXER MODEL

The turbulent mixer model considers the concentration variance a superposition of the variances in three subranges

$$\mathbf{s}_s^2 = \mathbf{s}_1^2 + \mathbf{s}_2^2 + \mathbf{s}_3^2 \quad (7)$$

where \mathbf{s}_1^2 , \mathbf{s}_2^2 and \mathbf{s}_3^2 are the inertial-convective, viscous-convective and viscous-diffusive concentration variances respectively. The subrange-variances satisfy the following transport equations

$$\frac{D\mathbf{s}_1^2}{Dt} = \frac{\partial}{\partial x_i} \left[(D_M + D_T) \frac{\partial \mathbf{s}_1^2}{\partial x_i} \right] + 2D_T \left(\frac{\partial \langle f \rangle}{\partial x_i} \frac{\partial \langle f \rangle}{\partial x_i} \right) - \mathbf{s}_1^2 R \frac{\langle \mathbf{e} \rangle}{k} \quad (8)$$

$$\frac{D\mathbf{s}_2^2}{Dt} = \frac{\partial}{\partial x_i} \left[(D_M + D_T) \frac{\partial \mathbf{s}_2^2}{\partial x_i} \right] + \mathbf{s}_1^2 R \frac{\langle \mathbf{e} \rangle}{k} - E\mathbf{s}_2^2 \quad (9)$$

$$\frac{D\mathbf{s}_3^2}{Dt} = \frac{\partial}{\partial x_i} \left[(D_M + D_T) \frac{\partial \mathbf{s}_3^2}{\partial x_i} \right] + E\mathbf{s}_2^2 - G\mathbf{s}_3^2 \quad (10)$$

where $R = 1.86$ is the velocity-to-scalar time-scale ratio. The engulfment parameter is given by $E = 0.058 \cdot \sqrt{\langle \mathbf{e} \rangle / \mathbf{n}}$ and the molecular diffusion parameter $G = (0.303 + 17050 Sc^{-1})E$.

THE SPECTRAL RELAXATION MODEL

In the spectral relaxation model there are three main subranges: 1) Transport from the lowest wavenumber to the integral wave-number representing the large energy-containing eddies, 2) further transport to the Kolmogorov scale and finally 3) transport from the Kolmogorov scale to the Batchelor scale. These subranges, referred to as i , are further divided into substages j . The ‘potential’ scalar dissipation in the j ’th substage in the i ’th subrange is denoted by $\langle \mathbf{e}_{i,j} \rangle$. The number of substages is determined by the Schmidt number and the turbulence Reynolds number, Re_λ , according to guidelines given by Fox². In the current work three substages were used for subrange two and one for subrange three. There is no first subrange in the present work. The ‘potential’ scalar dissipations are given by the following equations:

$$\frac{D\langle \mathbf{e}_{2,1} \rangle}{Dt} = \frac{\partial}{\partial x_i} \left[(D_M + D_T) \frac{\partial \langle \mathbf{e}_{2,1} \rangle}{\partial x_i} \right] + 2 \frac{C_w}{C_c - 1} \left(\frac{\langle \mathbf{e} \rangle}{\mathbf{n}} \right)^{1/2} D_T \left(\frac{\partial \langle f \rangle}{\partial x_i} \frac{\partial \langle f \rangle}{\partial x_i} \right) - \frac{2}{t_{2,1}} \langle \mathbf{e}_{2,1} \rangle \quad (11)$$

$$\frac{D\langle \mathbf{e}_{2,2} \rangle}{Dt} = \frac{\partial}{\partial x_i} \left[(D_M + D_T) \frac{\partial \langle \mathbf{e}_{2,2} \rangle}{\partial x_i} \right] + \frac{2}{t_{2,1}} \langle \mathbf{e}_{2,1} \rangle - \frac{2}{t_{2,2}} \langle \mathbf{e}_{2,2} \rangle \quad (12)$$

$$\frac{D\langle \mathbf{e}_{2,3} \rangle}{Dt} = \frac{\partial}{\partial x_i} \left[(D_M + D_T) \frac{\partial \langle \mathbf{e}_{2,3} \rangle}{\partial x_i} \right] + \frac{2}{t_{2,2}} \langle \mathbf{e}_{2,2} \rangle - \frac{2}{t_{2,3}} \langle \mathbf{e}_{2,3} \rangle \quad (13)$$

$$\frac{D\langle \mathbf{e}_{3,1} \rangle}{Dt} = \frac{\partial}{\partial x_i} \left[(D_M + D_T) \frac{\partial \langle \mathbf{e}_{3,1} \rangle}{\partial x_i} \right] + \frac{2}{t_{2,3}} \langle \mathbf{e}_{2,3} \rangle - \frac{2}{t_{3,1}} \langle \mathbf{e}_{3,1} \rangle \quad (14)$$

$$\begin{aligned} \frac{D\langle \mathbf{e}_f \rangle}{Dt} = & \frac{\partial}{\partial x_i} \left[(D_M + D_T) \frac{\partial \langle \mathbf{e}_f \rangle}{\partial x_i} \right] + \frac{2}{t_{3,1}} \langle \mathbf{e}_{3,1} \rangle + 2C_w \left(\frac{\langle \mathbf{e} \rangle}{\mathbf{n}} \right)^{1/2} \langle \mathbf{e}_f \rangle - \\ & \frac{4C_c}{2 + Sc^{-1}} \left(\sum_{i=1}^3 \frac{\langle \mathbf{e}_{2,i} \rangle}{\langle f' \rangle^2} + \frac{\langle \mathbf{e}_{3,1} \rangle}{\langle f' \rangle^2} + \frac{\langle \mathbf{e}_f \rangle}{\langle f' \rangle^2} \right) \langle \mathbf{e}_f \rangle \end{aligned} \quad (15)$$

where $C_c = 3$ and $C_w = 0.54$ are model constants.

The time constants are given by the following:

$$t_{2,1} = \frac{k}{\langle \mathbf{e} \rangle} - \left(\frac{\mathbf{n}}{\langle \mathbf{e} \rangle} \right)^{1/2}, \quad t_{2,2} = \frac{1}{3} t_{2,1}, \quad t_{2,3} = \frac{1}{2} t_{2,2}, \quad t_{3,1} = \frac{1}{2} \ln(Sc) \left(\frac{\mathbf{n}}{\langle \mathbf{e} \rangle} \right)^{1/2}$$

EXPERIMENTAL SETUP

Experiments were performed in a tubular mixer containing distilled water (see figure 1). An injection pipe for the fluorescent tracer rhodamine B (dissolved in distilled water) was concentrically located in the tube. The larger tube, made out of plexiglass with an inner diameter of 0.032 m, was placed so that the inlet was located 2.0 m before the injection point and outlet 2.0 m after. To reduce optical distortion, a rectangular plexiglass vessel filled with

distilled water surrounded the large pipe in the measuring area. The injection tube, made of stainless steel, had an inner diameter of 1.9×10^{-3} m, an outer diameter of 2.5×10^{-3} m and was 0.25 m long. Injection was controlled by a piston pump to achieve the highly accurate flowrate of $1.64 \times 10^{-6} \text{ m}^3 \text{ s}^{-1}$ for all experiments. Experiments were performed at four different Reynolds numbers ($Re=18500, 37000, 55500$ or 66600) in the main pipe. The laser used in the experiments was a pulsed Nd:YAG laser with the following characteristics: 10 W, 2 mJ per pulse, pulsewidth 20 ns and emission wavelength at 532 nm. The laser sheet had a gaussian intensity distribution that was accounted for in the postprocessing by normalizing all images with images obtained at uniform dye concentration. Images of size 256×240 pixels were captured with a 8-bit CCD-camera with frequency of 1000 fps. The size of a single pixel was equal to 25.7×10^{-6} m. During one experiment 4300 images were captured, which was considered enough to obtain fairly smooth concentration fields.

The thickness of the planar laser sheet was estimated to 0.6×10^{-3} m. Total measuring volume represented by one pixel in one image was thus $(0.0257 \times 0.0257 \times 0.6) \times 10^{-9} \text{ m}^3$. The main flow, with the injected rhodamine, was recirculated. To keep the background dye concentration at a minimum a large buffer tank containing near 1 m^3 of distilled water was placed in the loop. The water was replaced when the background concentration became detectable.

NUMERICAL SIMULATION

Numerical simulations were performed with the commercial software FLUENT 6.0.12 for computational fluid dynamics (CFD). Simulations were two-dimensional and axisymmetric. In simulations only the last 0.24 m before and 1.2 m after the injection point were calculated. Two different models were used for calculating the turbulent velocity field. The standard $k-\epsilon$ model (Launder and Spalding¹⁷) for homogeneous flows and the $k-\omega$ model of Wilcox¹⁸. Both models were used in the standard high-Reynolds number form.

Meshing of the pipe is far from trivial and can seriously affect the results. Most earlier works on the pipe injection in a tube has employed high-Reynolds number turbulence models with standard wall functions for near wall turbulence calculations (Ba³dyga et al.¹³; Marchisio, Fox et al.¹⁹; Hannon, Hearn et al.²⁰). The purpose of this work is to test two high-Reynolds number mixing models and thus it makes sense to adapt the same procedure here. A mesh that gives near wall y^+ -values higher than 30 is then needed. This is impossible to achieve for the lowest Reynolds number flow without severely compromising the numerical accuracy in the injection region by using a too coarse mesh. Another option is then to calculate this flow with a fully resolved boundary layer. Considering that the turbulence models are high-Reynolds number models that cannot be expected to describe this low-Reynolds flow well, the standard wall functions with too low y^+ -value is still chosen. Turbulent and laminar velocity profiles were set for the main and injection pipe respectively. Diffusion terms were discretized with second-order central differencing, whereas the convective terms were discretized by the QUICK-scheme (see FLUENT²¹). Pressure-velocity coupling was handled by the SIMPLEC scheme (see FLUENT²¹). The square mesh that was used for all calculations had the following cells in four different zones (radial \times axial): 1) Injection pipe zone with (6×192) equal square cells. 2) Zone surrounding the injection pipe with (24×192) equal square cells. 3) Area after the injection point (from 0.24 to 0.48 m) with (33×192) square skewed cells. The ratio of the length of the cell at the injection point relative to the outlet of the zone was 2:25. 4) Outlet area (from 0.48 to 1.2 m) with (33×216) equal cells.

RESULTS AND DISCUSSION

The linear relationship between rhodamine B concentration and fluorescence intensity was determined by performing several measurements at different concentrations directly at the injection point with near zero velocity of the main flow. By sampling 100 images at each concentration the linear regime was found to stretch to $600 \times 10^{-6} \text{ kg m}^{-3}$ (see figure 2). In later experiments the tracer concentrations in the injection were kept such that the maximum concentrations in all images were within the linear regime. Post-processing of the images was performed in MATLAB 6.0. Before statistics were calculated the images were filtered with a median filter. This filter was chosen because it efficiently removes noise and conserves the sharpness of the image.

One pixelsize ($2.57 \times 10^{-5} \text{ m}$) is about the size of the Kolmogorov scale ($\sim 10^{-5} \text{ m}$) for the high-Reynolds number experiments. This means that concentration fluctuations on the finest scales (from the Kolmogorov scale to the Batchelor scale) are filtered. However, the real limit in the measurements concerns the thickness of the laser sheet (estimated to the size of 23 pixels). There is no way of estimating the variance at scales smaller than one pixel without using a smaller measuring volume. However, it is possible to make some estimations of the effect of the sheet thickness on the measured variance, compared to what would have been obtained if all directions of the measuring volume had the size of one pixel (measuring volume of $1 \times 1 \times 1$ pixels). The error will be related to how much of the concentration fluctuations that are filtered. This will be a function of the sheet thickness compared to the integral lengthscale. The integral length scale near the injection point will be the diameter of the injection pipe. This scale will then grow towards the integral lengthscale of the main flow (diameter of main pipe) as we move downstream (Ba³dyga et al.¹⁶). Thus the error related to the measuring volume will be largest in the injection region and smaller downstream. A rough estimate of the variance that would have been obtained with a measuring volume of $1 \times 1 \times 1$ pixels can be found by extracting information from a larger measuring volume. Two different variances were calculated for measuring volumes of $1 \times 1 \times 23$ and $1 \times 23 \times 23$ pixels (both radial directions filtered). The variance at $1 \times 1 \times 1$ was then estimated as the square of the variance at $1 \times 1 \times 23$ divided by the variance at $1 \times 23 \times 23$ (by assuming that the ratio of variances at $1 \times 1 \times 1$ to $1 \times 1 \times 23$ equals the ratio of variances at $1 \times 1 \times 23$ to $1 \times 23 \times 23$). Using this extrapolation procedure it was estimated that the concentration variance should be about 25% higher near the injection and somewhat less far field $\sim 20\%$ (indicating an increase in the integral lengthscale). For this extrapolation procedure it was assumed that the laser intensity was uniform across the sheet thickness and that on the centreline the radial concentration distribution was identical to the distribution across the sheet thickness. Also the small difference in average covariance for the two measurement volumes was neglected. The estimate is probably a few percent too high due to an unknown gaussian laser intensity profile across the sheet thickness. However, a more precise estimate is not possible without exactly knowing the intensity profile and calculating the covariances between pixels.

Another important systematic error is the instability of the laser intensity. This error, which leads to an increase of the measured variance, was measured to be approximately $(3 \pm 0.5) \%$. It is worth mentioning that the systematic errors only apply to the concentration variances. Experimental concentration fields should be very accurate. Deviations here are most likely due to inaccurate placement of the laser sheet or inaccurate rhodamine concentration. Errors in the calculated concentration fields are due to erroneous turbulent viscosity and the fact that the Reynolds averaged turbulence models cannot detect the anisotropy in the injection region. Mean concentrations obtained at the centreline of the pipe are shown in figure 3 for different Reynolds numbers in the main pipe. Also the concentrations calculated with eq. (3) for two different turbulence models are shown.

Concentration variances at the centreline are shown in figure 4 and figure 5. Also shown are predictions by the two multi-scale models (TMM and SRM) combined with the two turbulence models ($k-\varepsilon$ and $k-\omega$). Figure 4 shows the area immediately after injection to get an idea of the peak variances, whereas figure 5 give a good presentation of the variance dissipation far from the injection point.

From figures 3 to 5 it is clear that neither the $k-\varepsilon$ nor the $k-\omega$ model can describe the flow at the two lowest Reynolds numbers. This is a clear indication that the flow is not fully turbulent in these experiments and a low-Reynolds turbulence model should have been employed instead. If the flow is not fully turbulent the mixing models cannot be expected to perform well.

In the following only the two experiments with highest Reynolds number are further discussed. Both turbulence models predict the axial position of the maximal concentration variance to within 4 mm. The predicted peak variance is larger with the $k-\omega$ model than with the $k-\varepsilon$ model due to the higher predicted mean concentration gradients immediately after injection (see figure 3). Maximum concentration variances seem to be estimated best by the $k-\varepsilon$ model together with the SRM model. It can be seen from figure 5 that the SRM- $k-\varepsilon$ combination also seems to give the best prediction of the axial variance profile as the calculated curves closely follow the experimental. The TMM- $k-\varepsilon$ combination predicts variances that are 2-3 times higher than the SRM- $k-\varepsilon$ far from the injection point. This is mainly due to a higher scalar dissipation predicted by the SRM for the injection region and the large difference in the models timescales for mixing on scales lower than the Kolmogorov scale. The viscous convective timescale E^{-1} in TMM is about 10 times higher than $0.5t_{3,1}$ in SRM.

It is not fair to compare the mixing models directly to the measured data as the mixing models contain information on scales smaller than what is detectable with the current system. A mixing model that only considers mixing from the integral to the Kolmogorov scale (homogeneous on smaller scales) should be more directly comparable. A nice feature with the TMM is that this information is directly available as the variance is considered a superposition of the variances at the different scales. The variance \mathbf{s}_1^2 , which describes inertial-convective subrange, gives a much better fit than the totally calculated variance and with the $k-\varepsilon$ model it is from 30 to 40 % lower than the experimental variance. It is also possible to use the SRM with scales smaller than the Kolmogorov scale removed. Equation (14) is then removed and $t_{2,3}$ is used instead of $t_{3,1}$ in equation (15). The differences in the calculated results are small, which shows that the SRM predict little fluctuations on scales lower than the Kolmogorov scale. This is in sharp contrast to the TMM. Again this is explained by the difference in E^{-1} and $0.5t_{3,1}$. The large value of E^{-1} leads to an accumulation of variance at the meso-scale, \mathbf{s}_2^2 in the TMM. The very good fit of the scalar relaxation model is explained by the fact that the model hardly predicts any fluctuations on scales smaller than the Kolmogorov scale. Such fluctuations are filtered by the experiments and thus the results should be comparable.

Distributions of concentration at some chosen points on the centreline are shown in figure 6. Also shown is the beta-PDF calculated from the experimental mean and variance at the point of interest. The beta-function is given by

$$\phi(f) = \frac{f^{v-1} (1-f)^{w-1}}{\int_0^1 x^{v-1} (1-x)^{w-1} dx} \quad (16)$$

where

$$v = \langle f \rangle \left[\frac{\langle f \rangle (1 - \langle f \rangle)}{\sigma_s^2} - 1 \right] \text{ and } w = v \frac{(1 - \langle f \rangle)}{\langle f \rangle} \quad (17)$$

There is a remarkable resemblance between the experimental distribution and the beta-function. More experimental points (more images) are necessary for very accurate experimental PDFs. The authors will present more results on concentration distributions in the pipe in later works.

CONCLUSIONS

Planar laser induced fluorescence has been used to study the concentration field of a passive tracer injected in the center of a pipe carrying intermediate to fully turbulent flows. Experimental results have been compared to CFD-calculations of two multiple-time-scale mixing models for the concentration variance. The scalar relaxation model (Fox²) is found to produce results that are in closer agreement with experiments than the turbulent mixer model (Ba³dyga¹). The very good fit of the scalar relaxation model is explained by the fact that the model hardly predicts any fluctuations on scales smaller than the Kolmogorov scale. Such fluctuations are also filtered by the experiments and thus the results should be comparable. The turbulent mixer model predicts more of the fluctuations to be on scales smaller than the Kolmogorov scale, which explains why the predicted variances are much higher than experiments. The beta-PDF, which is commonly used in chemical reaction rate modeling, is found to accurately describe the concentration distributions on the centerline of the pipe. PLIF has been found to be a very useful tool for non-intrusive measurements of concentration fields of a passive tracer.

NOMENCLATURE

- C = Concentration in eq. (1) [kg m^{-3}]
- C_c = Constant in SRM, $C_c = 3$
- C_w = Constant in SRM, $C_w = 0.54$
- D_M = Molecular diffusion coefficient [$\text{m}^2 \text{s}^{-1}$]
- D_T = Turbulent diffusion coefficient [$\text{m}^2 \text{s}^{-1}$]
- E = Engulfment parameter [s^{-1}]
- f = Dimensionless tracer (scalar) concentration [-]
- G = Molecular diffusion parameter [s^{-1}]
- I = Fluorescence intensity [Counts]
- k = Turbulent kinetic energy [$\text{m}^2 \text{s}^{-2}$]
- R = Velocity-to-scalar timescale ratio [-]
- Sc = Schmidt number [-]
- Sc_T = Turbulent Schmidt number [-]
- t = Time [s]
- $t_{i,j}$ = Time constants in SRM [s]
- v, w = Parameters in the beta-PDF [-]
- z = Axial distance from the injection point [m]
- ϕ = Beta-PDF [-]
- \mathbf{e} = Turbulent energy dissipation rate [$\text{m}^2 \text{s}^{-3}$]
- \mathbf{e}_f = Scalar dissipation [s^{-1}]

$\mathbf{e}_{i,j}$ = 'Potential' scalar dissipation [s^{-1}]

Γ_1 = Constant in eq. (1) [Counts $kg^{-1} m^3$]

Γ_2 = Constant in eq. (1) [$kg^{-1} m^3$]

\mathbf{s}_s^2 = Scalar concentration variance [-]

\mathbf{s}_1^2 = Variance for inertial-convective subrange [-]

\mathbf{s}_2^2 = Variance for viscous-convective subrange [-]

\mathbf{s}_3^2 = Variance for viscous-diffusive subrange [-]

μ_T = Turbulent dynamic viscosity [Pa s]

\mathbf{n} = Kinematic viscosity [$m^2 s^{-1}$]

$\langle \rangle$ = Averaged value

' = Fluctuation

REFERENCES

1. Ba³dyga, J. (1989). "Turbulent mixer model with application to homogeneous, instantaneous chemical reactions." Chem. Eng. Sci. **44**: 1175-1182.
2. Fox, R. O. (1995). "The spectral relaxation model of the scalar dissipation rate in homogeneous turbulence." Phys. Fluids **7**: 1082-1094.
3. Rhodes, R. P. (1975). "A probability density function for turbulent flows." in "Turbulent Mixing in Nonreactive and Reactive Flows." edited by S. N. B. Murthy, Plenum Press, New York: 235-241.
4. Frankel, S. H., Madnia, C. K. and Givi, P. (1991). "Modelling of the unmixedness in homogeneous reacting turbulence." Chem. Eng. Commun. **104**: 117-125.
5. Madnia, C. K., Frankel, S. H. and Givi, P. (1991). "Direct numerical simulations of the unmixedness in a homogeneous reacting turbulent flow." Chem. Eng. Commun. **109**: 19-29.
6. Li, K. T. and Toor, H. L. (1986). "Chemical indications as mixing probes. A possible way to measure micromixing simply." Ind. Eng. Chem., Fundam. **25**: 719-723.
7. Bilger, R. W. (1989). "Turbulent diffusion flames." Annual Review Fluid Mechanics **21**: 101-135.
8. Houcine, I., Marcant, B., Vivier, H., Plasari, E., David, R. and Villermaux, J. (1994). "Comparison of mixing action of several stirrers by laser sheet visualization and image processing." in proceedings of Eighth European Conference on Mixing, Cambridge, IChemE Symp Ser.
9. Houcine, I., Vivier, H., Plasari, E., David, R. and Villermaux, J. (1996). "Planar laser induced fluorescence technique for measurements of concentration fields in continuous stirred tank reactors." Exp Fluids **22**: 95-102.
10. Eckbreth, A. C., (1997). "Laser diagnostics for combustion temperature and species" 2 ed., Gordon and Breach Publishers, Amsterdam.
11. Guiraud, P., Bertrand, J. and Costes, J. (1990). "Laser measurements of local velocity and concentration in a turbulent jet-stirred tubular reactor." Chem. Eng. Sci. **46**: 1289-1297.
12. Kruis, F. E. and Falk, L. (1996). "Mixing and reaction in a tubular jet reactor: A comparison of experiments with a model based on a prescribed PDF." Chem. Eng. Sci. **51**: 2439-2448.
13. Ba³dyga, J. and Henczka, M. (1997). "Turbulent mixing and parallel chemical reactions in a pipe." Récents Progres en Génie des Procédés **11**: 341-348.
14. Heinz, S. and Roekaerts, D. (2001). "Reynolds number effects on mixing and reaction in a turbulent pipe flow." Chem. Eng. Sci. **56**: 3197-3210.
15. Ba³dyga, J. and Orciuch, W. (2001). "Barium Sulphate precipitation in a pipe - an experimental study and CFD modelling." Chem. Eng. Sci. **56**: 2435-2444.
16. Ba³dyga, J. and Bourne, J. R. (1999). "Turbulent Mixing and Chemical Reactions", Wiley, New York.
17. Launder, B. E. and Spalding, D. B. (1972). "Lectures in Mathematical Models of Turbulence", Academic Press, London.
18. Wilcox, D. C. (1998). "Turbulence Modeling for CFD", DCW industries, inc., La Canada, California.
19. Marchisio, D. L., Fox, R. O., Barresi, A. A. and Baldi, G. (2001). "On the Comparison between Presumed and Full PDF Methods for Turbulent Precipitation." Ind. Eng. Chem. Res. **40**: 5132-5139.

20. Hannon, J., Hearn, S., Marshall, L. and Zhou, W. (1998). "Assessment of CFD approaches to predicting fast chemical reactions." in proceedings of Chemical and Biological Reactors, Miami.

21. FLUENT 6 User's Guide. Lebanon, New Hampshire

Figure 1 Schematic of the experimental set up.

Figure 2 Calibration curve for rhodamine B for the experimental system. Measurements (+). Linear interpolation (solid line).

Figure 3 Mean concentration profiles at the centreline of the pipe for different Reynolds numbers. Measurements (*). Predicted by k - ϵ model (solid line) and k - ω model (dash-dash).

Figure 4 Concentration variance for the injection region at the centreline of the pipe for different Reynolds numbers. Measurements (*). Predicted by k - ω with TMM (dash-dot), k - ω with SRM (dash-dash), k - ϵ with SRM (solid) and k - ϵ with TMM (dot).

Figure 5 Concentration variance at the centreline for all measured points at different Reynolds numbers. Measurements (*). Predicted by k - ω with TMM (dash-dot), k - ω with SRM (dash-dash), k - ϵ with SRM (solid) and k - ϵ with TMM (dot).

Figure 6 Experimentally determined PDFs at some axial positions on the centreline (bars) and beta-PDF calculated with the same first two moments (solid line). $Re = 55500$.

Fig.1.



Fig.2.

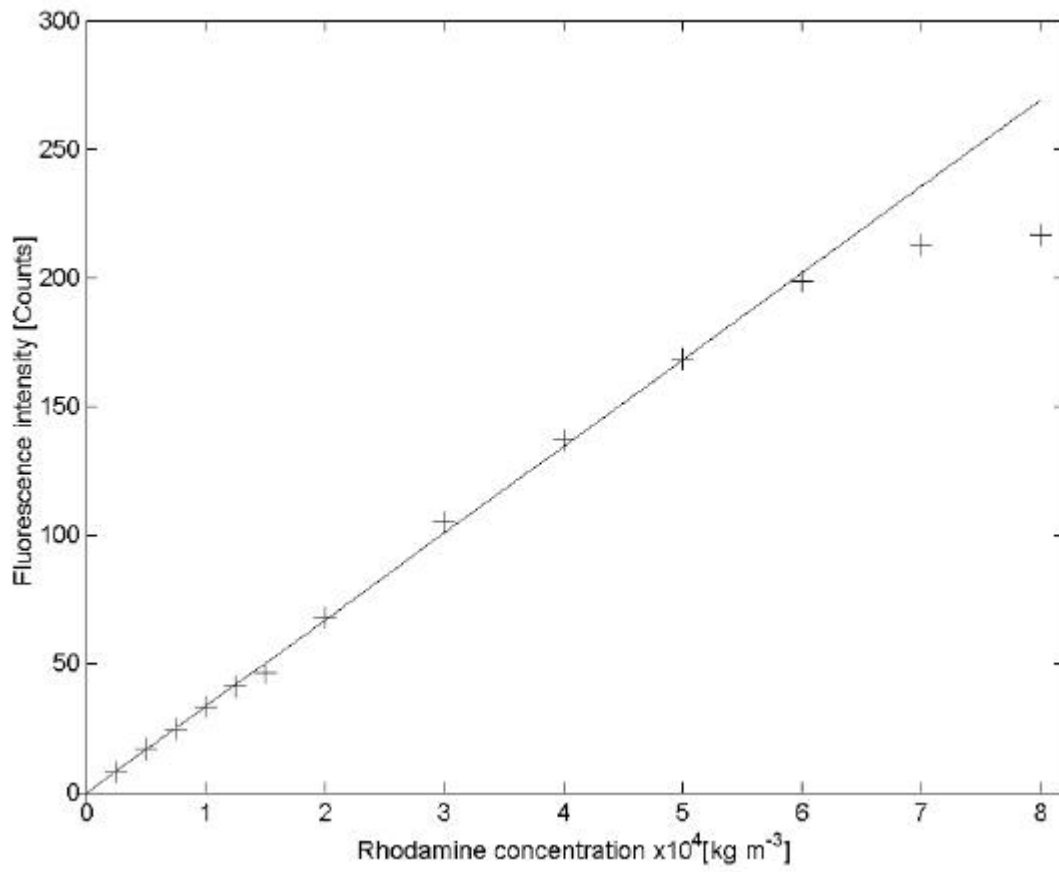


Fig.3.

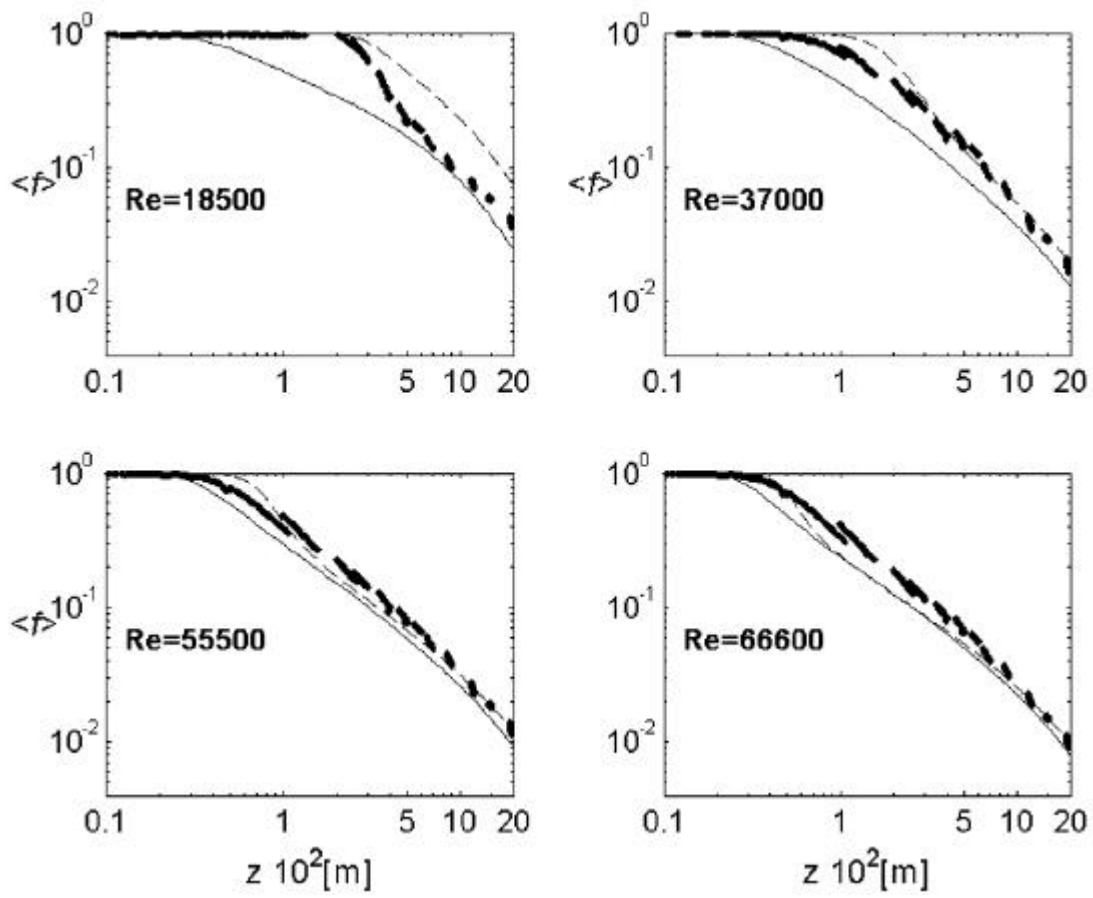


Fig.4.

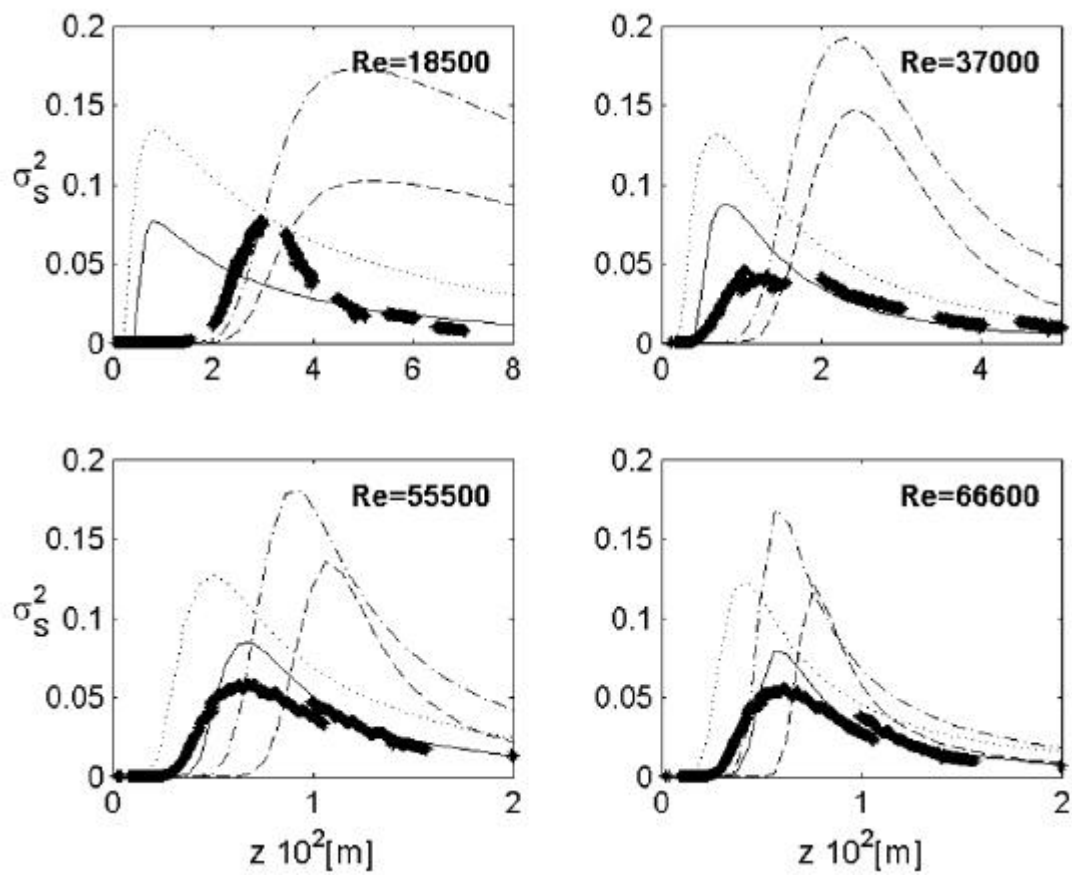


Fig.5.

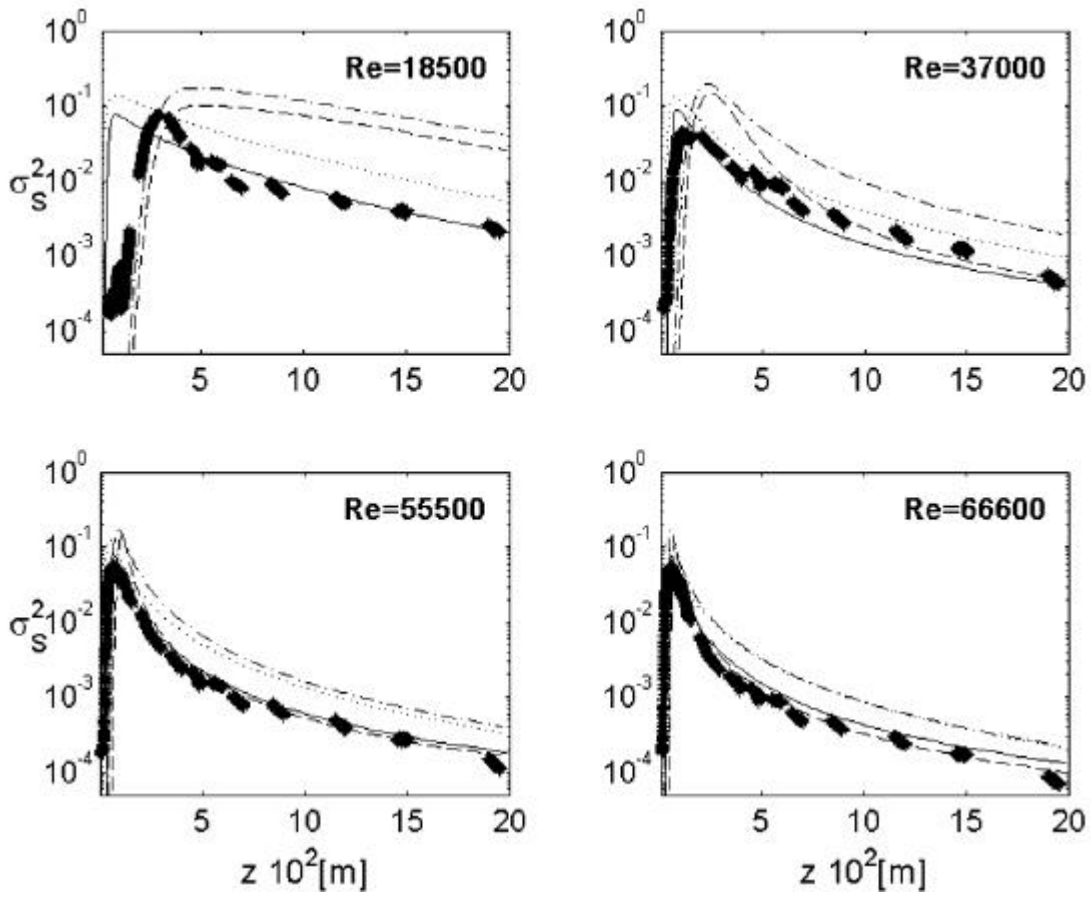


Fig.6.

